Journal of The
Electrochemical Society

Applicability of Graphene Oxide Interlayers in PEMs for Reducing Crossover in Electrochemical Acetone Hydrogenation Reactors

To cite this article: Miriam Komma *et al* 2024 *J. Electrochem. Soc.* **171** 104502

Journal of The Electrochemical Society, 2024 **171** 104502

Applicability of Graphene Oxide Interlayers in PEMs for Reducing Crossover in Electrochemical Acetone Hydrogenation Reactors

Miriam Komma,[1,2,=] Axel Marth,[1,2,=] Maximilian Maier,[1,2] Andreas Hutzler,[1] Thomas Böhm,[1] and Simon Thiele[1,2,z]

[1] *Forschungszentrum Jülich GmbH, Helmholtz Institute Erlangen-Nürnberg for Renewable Energy (IET-2), 91058 Erlangen, Germany*
[2] *Department of Chemical and Biological Engineering, Friedrich-Alexander-Universität Erlangen-Nürnberg, 91058 Erlangen, Germany*

Reactant and product crossover is challenging for proton exchange membrane (PEM)-based electrochemical systems, as it leads to efficiency losses and safety issues. Blocking interlayers can reduce the permeability of PEMs. In this work, a reduction in organic crossover by up to 55% is reached by implementing graphene oxide (GO) flakes in a Nafion membrane for application in an acetone hydrogenation reactor. Additionally, the GO-membrane's hydrogen crossover is reduced significantly. Those effects are accompanied by an up to 12% increased OCV and scale with the GO interlayer loading. The performance of the MEAs containing GO composite membranes is slightly reduced. This performance loss is traced back to an increased high-frequency resistance (HFR) of the GO composite membranes, the effect of an additional interface resistance resulting from the GO interlayer, and manufacturing-dependent variations in the electrochemically active surface area. Impedance analysis suggests a rearrangement of the GO flakes during operation, reflected by a decreasing HFR and interfacial resistance of the blocking interlayer after the net 15 h lasting electrochemical test protocol. This observation is supported by transmission electron microscopy, which shows structural variations in the GO interlayer at EoT. Nonetheless, the reduction in organic and hydrogen crossover is maintained at EoT.
 [DOI: 10.1149/1945-7111/ad7e54]

Manuscript submitted June 11, 2024; revised manuscript received September 16, 2024. Published October 3, 2024.

Supplementary material for this article is available online

Decarbonizing the world's energy sector is one of the main challenges for today's society. The turnaround from fossil fuels to carbon-neutral energy production can only be targeted with renewable energies. Using hydrogen as a chemical energy carrier is one strategy to achieve the goals of decarbonization.[1] A decentral storage of seasonal energy needs to be accomplished to close the loop besides the carbon-neutral production of hydrogen in water electrolysis with electricity from solar or wind power. There are different ways for storing the energy potential of hydrogen, for example, pressurized storage tanks,[2] metal hydride systems,[3] and liquid organic hydrogen carriers (LOHCs).[4–6] LOHCs are organic molecules that can take a hydrogen lean and hydrogen rich form. The hydrogen lean form can be hydrogenated with a surplus of hydrogen, thus becoming the hydrogen rich form. This hydrogen rich form can be dehydrogenated when hydrogen is needed, thus becoming the lean form again. The acetone/isopropanol couple is a promising candidate for LOHCs because it can not only be hydrogenated and dehydrogenated via thermal catalysis but also electrochemically in polymer electrolyte membrane (PEM) based reactors at significantly lower temperatures and ambient pressure.[4,5] Hydrogen is stored in the LOHC couple of acetone/isopropanol via the acetone hydrogenation. The full cell reaction as well as the anodic hydrogen oxidation reaction (HOR) and the cathodic acetone reduction reaction (ARR) of the acetone hydrogenation are provided in Eqs. 1–3.[5,7]

$$\text{Anode HOR: } H_2 \rightarrow 2H^+ + 2e^-;\ E^0 = 0\ \text{V vs. RHE} \quad [1]$$

$$\text{Cathode ARR: } 2H^+ + 2e^- + C_3H_6O \rightarrow C_3H_8O;\ E^0 = 0.118\ \text{V vs. RHE} \quad [2]$$

$$\text{Full cell: } C_3H_6O + H_2 \rightarrow C_3H_8O;\ E^0 = 0.118\ \text{V} \quad [3]$$

With a theoretical cell potential of 118 mV, an electrical current can be generated to reduce acetone to isopropanol in this electrochemical hydrogenation reactor. The product isopropanol can, for example, be utilized in a direct isopropanol fuel cell. In this setup the anode reaction is the isopropanol oxidation, and the cathode reaction is the oxygen reduction reaction. The overall reaction equals the hydrogen oxidation to water, with the acetone/isopropanol pair as a liquid energy carrier.[8,9]

One of the most severe problems of PEM-based electrochemical cells fed with liquid alcohol is the high fuel crossover, causing performance reduction due to mixed potential, reduced faradaic efficiency, and catalyst poisoning effects.[10–12] A high reactant and product crossover can be anticipated for the acetone hydrogenation reactor since perfluorinated sulfonic acids show a high uptake of alcohols.[13] Many interlayers have been implemented into PEMs to reduce their fuel crossover. The literature presents interlayers based on fibers,[14] inorganic 2D materials,[10,15] or other non-organic fillers.[16,17] For example, Lee et al.[16] implemented hexagonal boron nitride flakes into a PEM and, therewith, decreased the hydrogen crossover in a low-temperature PEM fuel cell notably. Breitwieser et al.[18] manufactured a fully spray-coated catalyst-coated membrane with a graphene oxide/cerium oxide interlayer and reported a reduced hydrogen crossover in a low-temperature PEM fuel cell. Single-layer graphene was implemented into PEMs for direct methanol fuel cells (DMFCs) by Yan et al.[15] and onto electrodes for DMFCs by Holmes et al.[10] Both works show a significantly reduced methanol crossover by the integration of this blocking layer. Also, a significant reduction in methanol crossover in a DMFC was shown by Chien et al.[12] with the incorporation of sulfonated GO flakes into a Nafion matrix. Gagliardi et al.[19] casted Nafion composite membranes containing 0.5 to 1.5 wt% GO flakes and, by evaluating the open circuit voltage (OCV) values in DMFC tests, found that the methanol crossover was reduced effectively by the GO flakes. They also detected a decrease in the proton conductivity of the GO composite membranes, which counteracts the benefits of a reduced methanol crossover and reduces the performance of a DMFC beyond a certain current density threshold.

Based on the effective suppression of methanol crossover by GO in the above-listed publications, this study aims to implement GO flakes into PEMs for application in an electrochemical acetone hydrogenation

[=] Equal Contribution.
[z] E-mail: si.thiele@fz-juelich.de

reactor as a model system for organic electrochemistry. Opposite to the above-mentioned study, the GO flakes are not homogeneously distributed in the membrane but sprayed as an interlayer between two commercial N211 Nafion membranes as a barrier layer for the reactant acetone, the product isopropanol, and hydrogen molecules. The resulting composite membranes are characterized in-depth by single-cell testing under different operating conditions as well as microscopically.

Experimental

Materials.—Nafion 211 (dry thickness 25 μm) and Nafion dispersion D2021 were purchased from Chemours (USA). Graphene oxide (5 mg ml^{-1} GO in water) was purchased from ACS Material LLC (USA). Isopropanol (>99.9% purity), 1-propanol (>99.5%), and acetone (>99.8%) were purchased at Merck (Germany) and used without further purification. For the anode, a Pt/C catalyst consisting of Vulcan XC-72 with Pt nanoparticles (40 wt%) with an average diameter of 2.7 nm (TEC10V40E catalyst from Tanaka, Japan) and for the cathode, a 40 wt% Pt-Ru/C catalyst on Vulcan XC-72 with an atomic Pt to Ru ratio of 1:1 (Fuel cell store, USA) was used. Gas diffusion layers H23 and H23C8 were ordered from Freudenberg (Germany). Glass fiber-reinforced PTFE gaskets and virgin PTFE were ordered from Hightechflon (Germany). For the hotpressing process, Pacopads were purchased from Pacothane Technologies (USA), and Kapton was ordered from CMC Klebetechnik (Germany). High-purity water, treated with a Milli-Q water purification system (18.2 MΩ, Merck, Germany), was used for ink manufacturing and cell tests.

Materials characterization.—A confocal Raman microscope (WITec alpha 300, Germany) was used to analyze the cross-section of the GO-Nafion composite sample. A 532 nm laser at 15 mW was employed with a water immersion objective (63x/1.0 W Plan-Apochromat, Zeiss, Germany) for signal acquisition. Confocal through-plane Raman scans were acquired with a width of 20 μm, a depth of 90 μm, and a pixel size of 0.66 μm in axial and lateral directions. The integration time per pixel was set to 40 ms. Spectra were recorded with a Peltier-cooled, back-illuminated EMCCD within a WITec UHTS300 VIS spectrometer with a 600 grooves mm^{-1} optical grating and a spectral center of 2200 cm^{-1}. Spectra were post-processed by shape-based background (shape size of 400) subtraction using the commercial software WITec Project Five+. Raman images are based on sum filters for GO (G-peak: 1515–1665 cm^{-1}) and Nafion (stretching mode of CF-bonds of the backbone: 700 to 760 cm^{-1}). Data from through-plane images were normalized with respect to the maximum intensity of the sample with 12 μg cm^{-2} loading.

Samples were prepared for transmission electron microscopy by embedding catalyst coated membranes in Araldite 502 epoxy resin (Science Services, Germany). After curing the resin, the samples were cut with a PowerTome PC (RMC Boeckeler, USA) using an ultra 45 diamond knife (Diatome, Switzerland). Ultra-thin sections at a nominal thickness of 100 nm were collected on lacey carbon-coated Cu grids (Plano, Germany).

High-angle annular dark field scanning transmission electron microscopy (HAADF-STEM) was performed using a Thermo Fisher Scientific Talos F200i operated at a primary electron energy of 200 keV. A beam current of 40 pA and a convergence angle of 10.5 mrad were used for imaging. Energy dispersive X-ray spectroscopy (EDXS) was performed using two Bruker XFlash 6T-100 EDS detectors. Prior to imaging, the samples were cleaned in a PIE Scientific Tergeo EM plasma cleaner utilizing an ambient air remote plasma to reduce carbon contamination.

Membrane fabrication.—The GO interlayer was implemented between two Nafion N211 membranes using spray-coating (Sonotek ExactaCoat, USA). For manufacturing the GO interlayer, a dispersion of 25 ml isopropanol (IPA) and 2.5 ml GO dispersion was sonicated for 30 min in an ultrasonic bath, sonicated for 1 min with an ultrasonic horn (10 W), and stirred overnight. Before spray-coating, another ultrasonication in the bath was conducted for 30 min. The following spraying parameters were utilized: 60 °C substrate holder temperature, 0.2 l min^{-1} flow rate, ultrasonic idle power of 2.0 W, and run power of 3.5 W. The GO loading of the interlayer was adjusted to 3, 6, and 12 μg cm^{-2} by measuring the weight increase per run of spray coating and adjusting the number of runs accordingly. After the spraying process, a second N211 membrane was hotpressed (Collin P200S, Germany) on top of the N211-GO composite membrane. The hotpressing procedure was conducted as follows: 120 °C, 1 min, 0.5 MPa; followed by a temperature and pressure ramp within 2.5 min to the 2nd step: 155 °C, 4 min, 2.5 MPa. Two N211 membranes were hotpressed with the same parameters as the reference system.

Decal electrode fabrication and MEA assembly.—The inks for the decal electrodes were produced with the Pt/C catalyst for the anodes and the Pt-Ru/C catalyst for the cathodes. To prepare both inks, an ionomer dispersion (Nafion D2021), water and 1-propanol were used additionally to the catalysts. The solid content of both inks was 13.5%. The I/C ratio was 0.65 and the water content of the dispersion was 10 wt% for both inks. ZrO_2 beads were added as a grinding medium, and the ink was mixed for 24 h at 60 rpm on a roller mill. The ink was spread on a 50 μm virgin PTFE substrate with the Mayer rod coating technique at a wet film thickness of 100 μm. After drying at room temperature, the electrodes were additionally dried at 60 °C for 1 h. After cutting in 5 cm^2 pieces, the decal electrodes were transferred to the membranes via hotpressing (1st step: 120 °C, 1 min, 0.5 MPa; followed by a temperature and pressure ramp within 2.5 min to the 2nd step: 155 °C, 4 min, 2.5 MPa). The electrodes used for the membrane electrode assemblies (MEAs) had a Pt/C loading of 0.30 ± 0.04 mg cm^{-2} and a Pt-Ru/C loading of 0.31 ± 0.03 mg cm^{-2}. The catalyst-coated membranes were assembled with the gas diffusion layers (H23 to the cathode and H23C8 to the anode) to form MEAs, which were mounted in the cell fixtures with 25% compression, adjusted by glass fiber-reinforced PTFE gaskets. The cell fixture was tightened with a torque of 5 Nm.

Acetone hydrogenation reactor tests.—All acetone hydrogenation reactor cell tests were conducted at a customized Scribner redox flow cell test station (Scribner Associates Inc., USA) equipped with a VSP-300 potentiostat from BioLogic SAS (France) and a pressurized liquid container with a mass flow controller from aDROP (Germany) to feed the cell with preheated organic reactant. The Scribner cell hardware consisted of a graphite flow field (5 cm^2) with a multi-serpentine-single-channel design, gold-coated current collectors, a hydrogen fuel cell endplate for the anode compartment, and a redox flow battery endplate for the cathode compartment. The pressurized liquid container was filled with the required molarity of acetone in DI water after degassing the reactant with 100 ml min^{-1} nitrogen for 15 min. A scheme of the experimental setup for the electrochemical analysis of the MEAs can be seen in Fig. 1. The cathode compartment was fed with acetone in a distinct molarity, and the cathodic exhaust line was connected to a three-neck-bottom flask that was fed with 25 ml min^{-1} nitrogen. The anode compartment was fed with humidified hydrogen (95% relative humidity). The anodic outlet was either directly led to the exhaust (Fig. 1 path 1) or transferred to a unit for the organic crossover determination and afterwards led to the exhaust. The concentration of organics in the hydrogen stream was obtained using a Dimroth cooler made of glass that was filled with cooled DI water (4 °C) and connected to the acetone hydrogenation rector's anode (hydrogen side) outlet to trap the organic in the water (see Fig. 1 path 2). Quantitative evaluation of the organic concentration in the water was conducted with a gas chromatograph via a flame ionization detector (GC; Clarus 590, PerkinElmer, Inc., USA).

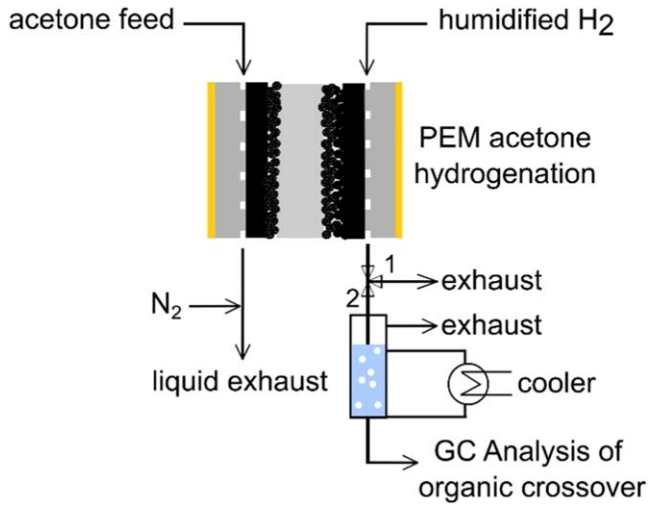

Figure 1. Scheme of the PEM-based electrochemical acetone hydrogenation reactor. The cathode compartment is fed with an acetone/DI water mixture of the required molarity with a flow rate of 7.5 ml min^{-1}. The liquid product isopropanol, not converted acetone, and crossover H_2 are collected in a three-neck bottom flask and diluted with 25 ml min^{-1} nitrogen. The anode compartment is fed with humidified hydrogen at a flow rate of 0.1 l min^{-1}, and the excess hydrogen is either transferred to the exhaust (1) or directed through a Dimroth cooler filled with chilled water (4 °C) to trap the organic crossover species (2). The concentration of the crossover organics is evaluated with a GC.

Electrochemical evaluation of the MEAs was performed for different temperatures ranging from 40 to 80 °C at a constant 1 M acetone feed concentration or with different concentrations ranging from 0.25 to 1 M at a constant temperature of 50 °C. The chronological order of the test procedure and additional information about the evaluated data can be found in the supporting information (Table S1 and Fig. S1). To ensure steady-state conditions, the acetone reactant was fed for 10 min, or alternatively, DI water was supplied for 15 min, each with 7.5 ml min^{-1}, before any electrochemical analysis was conducted. Between different temperatures or concentrations, leftover organics were flushed out of the cell by feeding DI water for 15 min at a feed rate of 7.5 ml min^{-1}. Cyclic voltammetry (CV) with a scan rate of 50 mV s^{-1} and an upper and lower vertex potential at 0.6 V and 0.07 V was utilized to determine the electrochemically active surface area (ECSA) of the electrodes at the begin and end of the test. Hydrogen crossover in water and acetone was determined electrochemically via voltage stepping (0.2–0.6 V) with a hold time of 2 min at each potential (last 30 s were averaged) while hydrogen was fed to the anode compartment at 0.1 l min^{-1} and water or acetone at the cathode side with 0 l min^{-1}. The intercept with the *y*-axis, corresponding to the hydrogen crossover current, was evaluated from these voltage stepping data. Additionally, potentiostatic electrochemical impedance spectroscopy (PEIS) measurements at 0.4 V under blocking conditions (potential range where no faradaic reaction is expected) were conducted in water and acetone (frequency range 500 kHz to 200 mHz, amplitude 3.5 mV). Before the voltage stepping, CV, and PEIS in water were performed, the water feed rate was set to 0 ml min^{-1}, and the water was degassed electrochemically by applying a cathodic current, thereby reducing leftover oxygen in the water.

The determination of the organic crossover from the cathode compartment (acetone, isopropanol) through the PEM into the anode compartment (hydrogen) was done by directing the anodic exhaust flow through 100 ml of cooled DI water (4 °C) and, therewith, collecting the crossover organics as depicted in Fig. 1 path 2. The organic crossover was determined under OCV conditions. The OCV was held for 15 min, the anodic exhaust was redirected through the cooled water, and the crossover organics concentration was analyzed with the GC. The permeation rate was determined according to Eq. 4 where $n_{crossover,\ organics}$ is the sum of the acetone and isopropanol amount of substance, t is the time of the measurement, and A corresponds to the active area of the cell, which was 5 cm^2 in all experiments.

$$J = \frac{n_{crossover,organics}}{t \cdot A} \quad [4]$$

Polarization curves were recorded galvanostatically in the current range of 10 mA cm^{-2} to 100 mA cm^{-2} with a hold time of 3 min each (the last 30 s were averaged). Furthermore, a 3 min hold at OCV conditions was conducted. Galvanostatic impedance measurements (GEIS) were performed at the corresponding currents or OCV in the frequency range of 500 kHz to 100 mHz with a 10% current amplitude (except for currents below 60 mA cm^{-2} where a fixed amplitude of 4 mA cm^{-2} was applied to ensure data quality) to determine the HFR by evaluation of the x-intercept. With the HFR values, the HFR-corrected polarization curve was determined according to Eq. 5. The polarization curves were acquired at a flow rate of 0.1 l min^{-1} hydrogen at the anode compartment and acetone in the cathode compartment with a flow rate of 7.5 ml min^{-1}.

$$E_{HFR\ corrected} = E + |i| \cdot HFR \quad [5]$$

While the CV and polarization curve measurements were only conducted at the beginning and end of the test at fixed parameters of 50 °C and 1 M acetone, the hydrogen crossover, PEIS, and organic crossover measurements were conducted in water and acetone at different temperatures and concentrations of the acetone feed.

Two MEAs of each type (incorporating the reference membrane or a composite membrane with the different GO loadings) were independently measured. The average values of the two measurements are shown with error bars based on the minimum and maximum.

Results and Discussion

The successful implementation of the GO interlayer between two N211 membranes was evaluated with confocal Raman microscopy by recording through-plane images. Additionally, to the through-plane evaluation elucidated in the following, the separated Raman spectra plots of GO and Nafion and a peak analysis of the characteristic signals are shown in the supporting information (see Fig. S2). The through-plane image results for 3, 6, and 12 μg cm^{-2} GO loading in the composite membrane can be seen in Fig. 2. The intensity distribution of the G band (1515–1665 cm^{-1}) of graphene shows the GO flake arrangement[20] in the different composite membranes, and the C-F stretching mode (700–760 cm^{-1}) depicts the Nafion fraction of the membrane.[21] The GO interlayer can be clearly detected in the middle of all composite membranes. Due to the diffraction-limited resolution of light microscopy, no variation in the GO interlayer thickness can be seen for increasing GO loading. Nevertheless, the intensity of the Nafion signal below the GO interlayer decreases for increasing GO loading. This phenomenon can be attributed to a stronger light attenuation by the interlayer with increasing GO loading, confirming the loading variation.

Figure 3 depicts the temperature- and concentration-dependent permeation rate of organics (acetone and isopropanol) from the cathodic to the anodic compartment for the reference MEA and the MEAs incorporating the three different loadings of GO flakes. As expected from the literature,[22,23] the permeation rate increases with temperature and concentration of the acetone reactant mixture independently of the measured MEAs. Generally, all three loadings of GO flakes in the composite membrane drastically reduce the

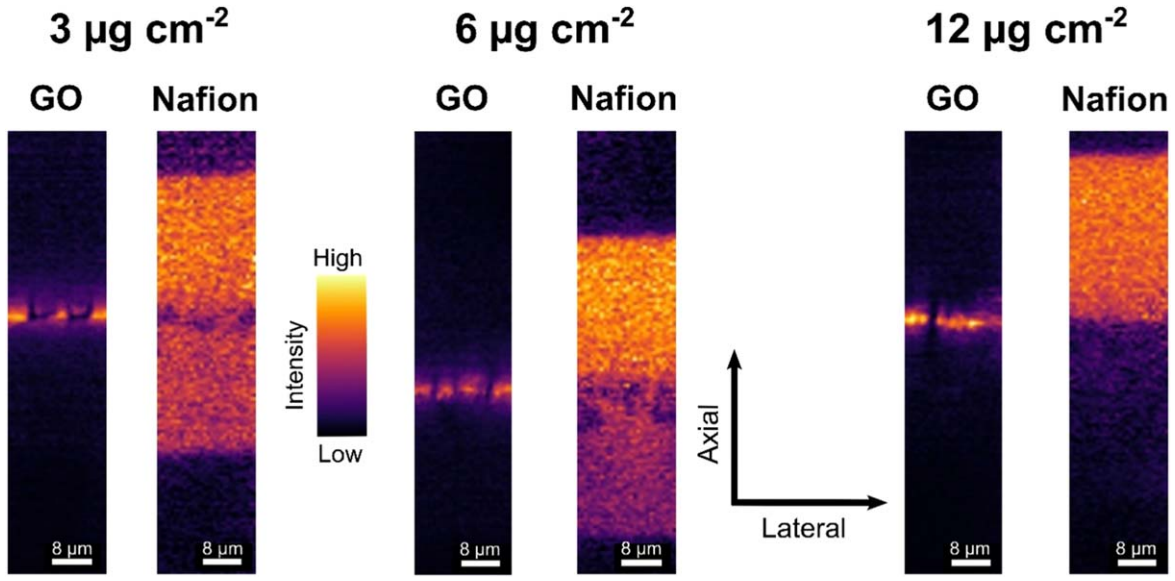

Figure 2. Sum filter images of the Raman through-plane scans of the GO interlayer Nafion membranes with a loading of 3 µg cm^{-2}, 6 µg cm^{-2}, and 12 µg cm^{-2}, acquired in water immersion. The intensity distribution is shown for the GO G-peak (1515–1665 cm^{-1}) and the C-F stretching mode of Nafion (700–760 cm^{-1}). The three images for the G-peak are normalized to the maximum intensity value of the 12 µg cm^{-2} loading, whereas each Nafion image is min-max normalized independently for each loading.

organic crossover through the PEM for measurements at different temperatures and concentrations. The data (Fig. 3a) also show that at low temperatures (40 °C), the decrease of organic crossover (around 40%–50%) through the implementation of GO flakes is relatively independent of the loading. With increasing the temperature, the reduction in the organic crossover is more pronounced for the GO interlayers with higher loadings of 6 and 12 µg cm^{-2}. While a GO loading of 3 µg cm^{-2} leads to an organic crossover reduction between 22% and 46% (60 °C–80 °C), a decrease of 46%–55% and 40%–49% is measured in the same temperature range for 6 and 12 µg cm^{-2}, respectively.

A similar trend can be seen for increased concentrations in the acetone feed (Fig. 3b). For example, the reduction in permeation reaches 32% for the 3 µg cm^{-2} sample at 0.25 M but the MEAs containing a composite membrane with 6 and 12 µg cm^{-2} GO flakes result in a permeation reduction of 54 and 43%, respectively. The same trend is visible for 0.5 M acetone mixtures but all three loadings result into a similar decrease of around 45% at 0.75 M. Since a further increase of the molarity from 0.75 M to 1 M acetone did not result in an increase of permeation rate for the reference and the 12 µg cm^{-2} MEAs for 1 M, but all other MEAs follow the trend expected from Fick's first law, we assume measurement deviations for these tests. Therefore, the permeation rate with increasing molarity was additionally measured with a third MEA for the reference, the 3 µg cm^{-2}, and the 12 µg cm^{-2} GO loaded MEAs (Fig. S3). The repetitions support the hypothesis of outliers in the data in Fig. 3b since they follow the expected trend. Summarized, a significant reduction in permeation by the implementation of the GO interlayer can be observed for all loadings at all tested concentrations, and the data hints toward a positive effect of organic crossover reduction by increasing the loading above 3 µg cm^{-2}.

In addition to the organic crossover, the crossover of hydrogen gas was determined to evaluate the effect of an interlayer in a PEM-based hydrogenation reactor. Similar to the decrease in organic crossover, a significant reduction in hydrogen crossover is observed by incorporating GO flakes (see Fig. 4). The effect scales with GO loading in the interlayer. While a GO loading of 3 µg cm^{-2} results in an H_2 crossover reduction (measured in acetone) of 15% at 60 °C, a decrease of 39% and 55% for 6 and 12 µg cm^{-2} is measured at the same temperature, respectively. Notably, the hydrogen crossover rate for all MEAs decreases with temperatures >60 °C when measured in acetone (Fig. 4a). We attribute this phenomenon to the thermally catalyzed hydrogenation of acetone with the crossover H_2 on the catalytically active Pt/Ru sites.[24] At elevated temperatures, a larger quantity of hydrogen is likely to react thermocatalytically with acetone on the catalyst, thus leading to isopropanol as a product. The H_2 participating in the thermal hydrogenation is not available for the electrochemical measurement of H_2 crossover, thus an apparent reduction of hydrogen crossover is observed at elevated temperatures. An additional partial electrochemical oxidation of isopropanol is unlikely to take place due to the inhibition by a large amount of acetone present at the catalyst sites since the cell is supplied with a pure acetone in water feed. Thus, we attribute no oxidative current for a partial dehydrogenation of isopropanol. To mitigate the effect of thermal hydrogenation, the H_2 crossover is additionally measured in water (Fig. 4b). In this procedure, the anticipated trend of increasing H_2 crossover with temperature can be detected for all measured MEAs, and the crossover reduction caused by the GO interlayer scales with loading. For instance, a highly reduced H_2 crossover rate is detected at 80 °C for the GO loadings of 6 and 12 µg cm^{-2}, with a 61% and 67% reduced permeation compared to the reference MEAs. In general, the H_2 permeation rates are higher for the crossover measurements in acetone than for the measurements conducted in water. We attribute this phenomenon to an increase in solvent sorption and swelling for the membrane in the acetone feed compared to the pure water feed, which is a known behavior for Nafion membranes.[13] Therefore, the permeation rate for H_2 is increased when measured in acetone. The authors assume higher absolute H_2 crossover rates than determined by the electrochemical measurement, due to the previously discussed thermal hydrogenation of acetone.

From the results mentioned above, it can be concluded that the GO interlayers are a highly efficient measure to reduce the permeation of organic species and H_2 molecules through the PEM for application in an acetone hydrogenation reactor.

Since the hydrogenation rate scales with the current density assuming constant Faradaic efficiency, the polarization behavior of all MEAs is characterized in Fig. 5 at begin of test (BoT). Figure 5a shows the uncorrected polarization curve and Fig. 5b depicts the HFR-free polarization data.

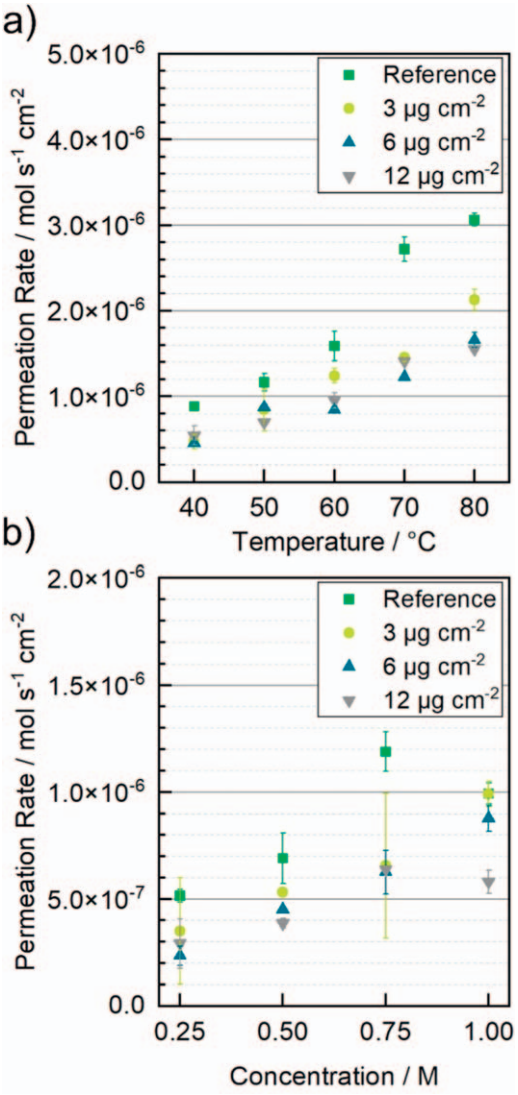

Figure 3. Temperature- and concentration-dependent permeation rate of organic species (acetone and isopropanol) from the cathodic (acetone-fed) compartment to the anodic (humidified hydrogen) compartment. The crossover of organics was determined during a 15 min hold at OCV with a flow rate of 0.1 l min^{-1} hydrogen and 7.5 ml min^{-1} of acetone at distinct temperatures with a fixed molarity of 1 (a) and with different molarities and a constant temperature of 50 °C (b). Depicted are the means of two MEAs for each data point, with the error bars indicating the minimum and maximum.

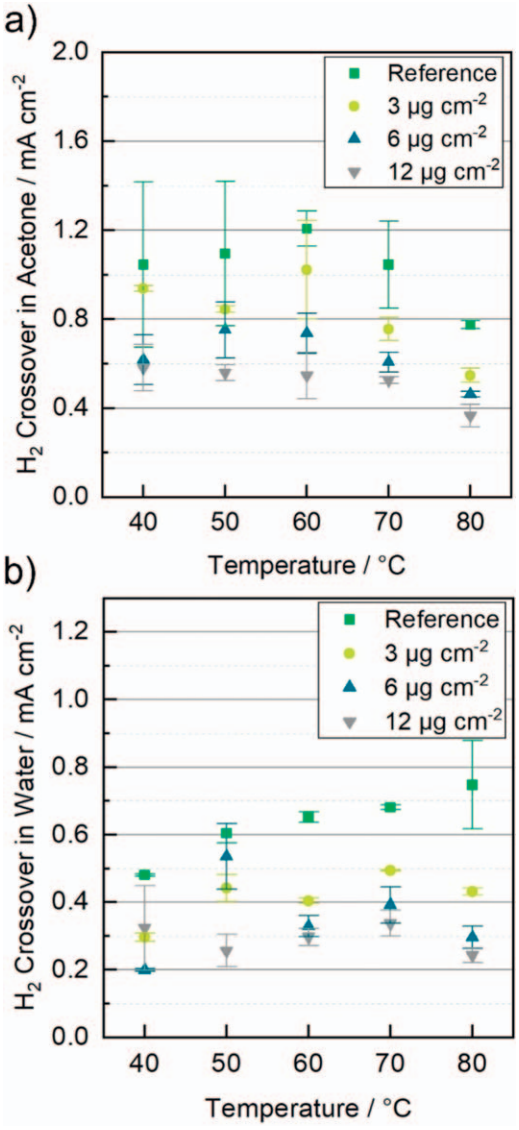

Figure 4. Temperature-dependent hydrogen crossover current from the anodic compartment (humidified hydrogen) to the cathodic compartment (acetone mixture (a) or DI water (b)). The crossover current was determined via voltage stepping at a flow rate of 0.1 l min^{-1} hydrogen and 0 l min^{-1} of 1 M acetone or DI water at different temperatures. Depicted are the means of two MEAs for each data point, with the error bars indicating the minimum and maximum.

A substantial increase in OCV for the MEAs containing GO composite membranes can be observed for all investigated loadings (see Table I, BoT). For example, an increase in OCV by up to 10% is achieved by the 6 µg cm^{-2} GO barrier layer. The rise in OCV is the electrochemical reflection of the previously shown reduction in crossover behavior for both hydrogen[25] and organic species.[10]

On the other hand, a performance decrease can be observed with increasing current densities for the MEAs containing the GO composite membranes. This effect can partially be explained by a considerable increase in the HFR of the GO composite membranes compared to the reference membrane, which results in an increase of the ohmic drop. An HFR correction was performed to investigate the data without the influence of the ohmic drop (Fig. 5b). However, the HFR does not fully explain the reduced performance of the MEAs containing GO interlayers. The measured HFR values in acetone at different temperatures and concentrations can be compared in Fig. 6. Independently of the temperature and concentration, the HFR of the GO composite membranes is increased by a factor of around 1.7 for the 3 µg cm^{-2} loading, and up to 2.0 and 2.3 for the 6 and 12 µg cm^{-2} samples, respectively. The reduction in HFR with increasing temperature (Fig. 6a) is due to the increase in proton conductivity of Nafion with rising temperature[26] and was also observed when measured in a pure water feed (Fig. S4), whereas the increase in HFR with increasing acetone concentration (Fig. 6b) can be explained by a more pronounced membrane swelling and decreased water fraction inside the membrane, leading to a reduction of proton conductivity.

An additional arc-shaped feature, often correlated to an RC element, in the impedance spectra of the GO composite membranes was discovered in the high-frequency region of the impedance spectra measured under blocking conditions, as depicted in Fig. 7. The characteristic of this feature increases with GO loading, which can be seen in the expansion of the additional arc to lower frequencies. Attempts to model this feature by a resistor-capacitor

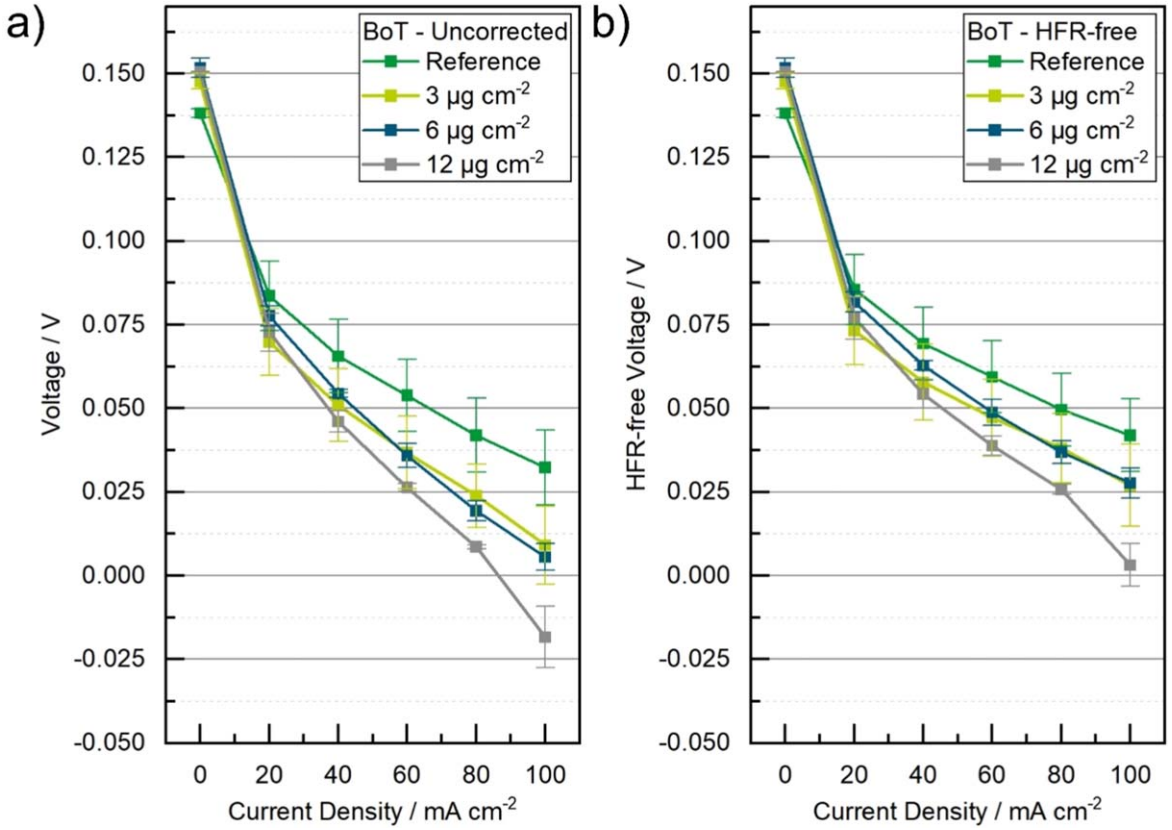

Figure 5. Uncorrected (a) and HFR-free polarization curves (b) at BoT for the reference and the three different GO interlayer loadings of 3, 6, and 12 μg cm^{-2}. The polarization data were acquired at 50 °C cell temperature, 1 M acetone, a flow rate of 0.1 l min^{-1} hydrogen, and 7.5 ml min^{-1} acetone feed. Depicted are the means of two MEAs for each data point, with the error bars indicating the minimum and maximum. A line between the single data points was added to guide the eye.

Table I. Summary of the OCV values measured during the polarization analysis at BoT and end of test (EoT) (Figs. 5 and 8). The polarization data were acquired at 50 °C cell temperature, 1 M acetone, a flow rate of 0.1 l min^{-1} hydrogen, and 7.5 ml min^{-1} acetone feed.

MEA	Reference	3 μg cm^{-2}	6 μg cm^{-2}	12 μg cm^{-2}
OCV_{BoT}/mV	138 ± 1	148 ± 2	152 ± 3	150 ± 0
OCV_{EoT}/mV	130 ± 1	140 ± 2	146 ± 1	146 ± 1

(RC) element caused by the additional interface of the GO blocking layer failed to satisfactorily fit the observed impedance spectra (see supporting information, Fig. S5). Hence, we opted to use the *x*-axis intercept as an approximation of the HFR. However, it must be noted that the additional RC element can influence the x-intercept and, therefore, possibly cause systematic offsets in the HFR value.

The HFR-free polarization curves indicate additional losses for the MEAs containing the GO composite membranes besides the ohmic drop (Fig. 5b). On the one hand, it has to be noted that the polarization curves are not corrected for the protonic sheet resistance in the electrodes since the influence of the organics on the catalyst utilization is unknown, and therefore, the established correction methods[27] cannot be applied. On the other hand, the decreased performance of the GO composite membrane MEAs can also be explained by comparing the ECSAs. The reference MEA shows a larger ECSA, which can be traced back to manufacturing variations in the decal process of the electrodes (see Table S2 and Fig. S6). It must be noted that the ECSA of the utilized Pt-Ru electrodes is only estimated with the area-specific charge capacity of Pt (210 μC cm^{-2}) since no values for alloys are known in the literature, thus an exact correction of the current based on the ECSA would be erroneous. This approach for calculating the ECSA of Pt-Ru alloys has also been used by other authors.[28,29] Furthermore, mass transport issues could also contribute to the decreased performance of the MEAs containing GO composite membranes. The GO interlayer reduces the permeation of the organic species through the PEM. While this effect is beneficial for the faradaic efficiency of the cells and results in an increased OCV, a negative effect on the cell potential at increasing current densities can be anticipated as a side effect: the hydrogenation product isopropanol may accumulate in the electrode, potentially causing a decreased availability of active sites for the acetone hydrogenation reaction. This hypothesis assumes, that isopropanol also permeates through the membrane, thus decreasing the amount of product on the cathode side. An increased permeation barrier would lead to a decrease of this effect, thus decreasing performance based on the equilibrium of reactant and product.

A comparison of the polarization behavior of the MEAs at BoT and EoT reveals that all three GO loaded MEAs show similar performance at EoT (Fig. 5 vs Fig. 8). Furthermore, the overall electrochemical performance of all tested MEAs, including the reference, increases. When comparing the differences at specific potentials, e.g., at 60 mA cm^{-2}, it can be noticed that the reference and 3 μg cm^{-2} MEAs show an increase in potential at EoT of about 13%–15%, while the 6 μg cm^{-2} and the 12 μg cm^{-2} MEAs display an increase in potential of 25 and 68%, respectively. This finding suggests a break-in process for all tested MEAs, which is supported by an increased ECSA by a factor of 1.4–1.8 at EoT determined from CV measurements after the acetone hydrogenation experiments (Table S2 and Fig. S5) for all tested MEAs. This phenomenon can be explained by a reduction of (hydrous) Pt-Ru oxides in the cathode catalyst layer[30] via hydrogen exposure during the evaluation of the

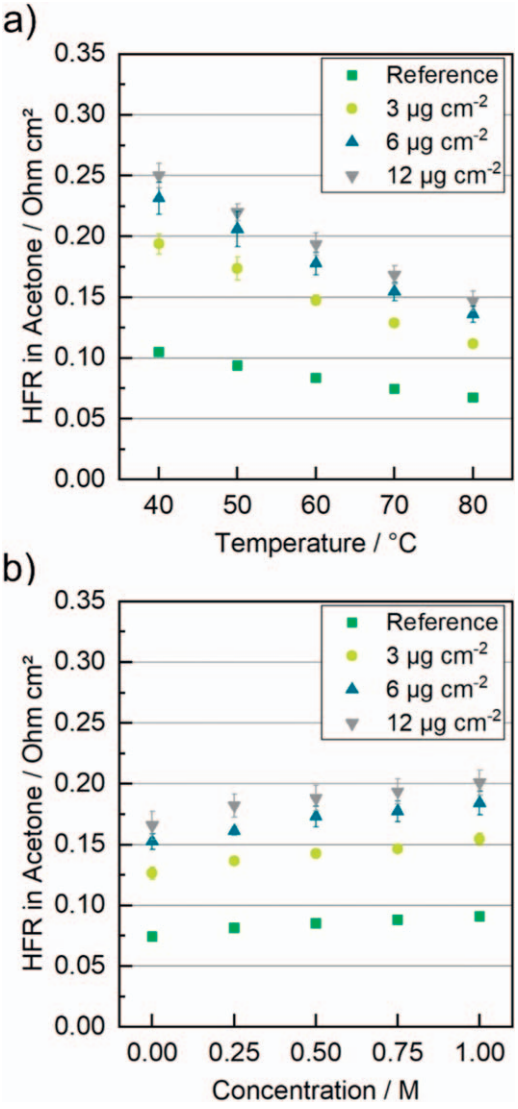

Figure 6. Temperature (a) and concentration-dependent (b) HFR values measured with 0.1 l min^{-1} hydrogen flow and 0 l min^{-1} acetone feed. For the temperature variation, a constant acetone molarity of 1, and for the concentration variation, a constant temperature of 50 °C were applied. Depicted are the means of two MEAs for each data point, with the error bars indicating the minimum and maximum.

MEAs. In general, a more substantial H_{upd} behavior is expected from metallic platinum-group metals than for the (hydrous) oxides since more metallic surface is available for desorption and adsorption. The reductive current under active conditions likely reduces any (hydrous) oxides inside the catalyst layer, similar to break-in procedures in PEMFCs, which then increase the performance.

Additionally, the conclusion can be drawn that the GO interlayer undergoes rearrangement, which especially impacts the composite MEAs with higher GO loading, as can be observed in the polarization data at EoT compared with BoT (Figs. 8, 5). This hypothesis is supported by a decrease in HFR in acetone and water of the MEAs incorporating GO interlayers, suggesting an alteration in the ionic pathways through the composite membrane (see Figs. 9a and S7). Furthermore, a decline of the additional RC feature in the impedance measurement is observed, which also strengthens this hypothesis (compare Figs. 9b and 7). It must be noted, that the organics acetone and isopropanol can additionally partially dissolve

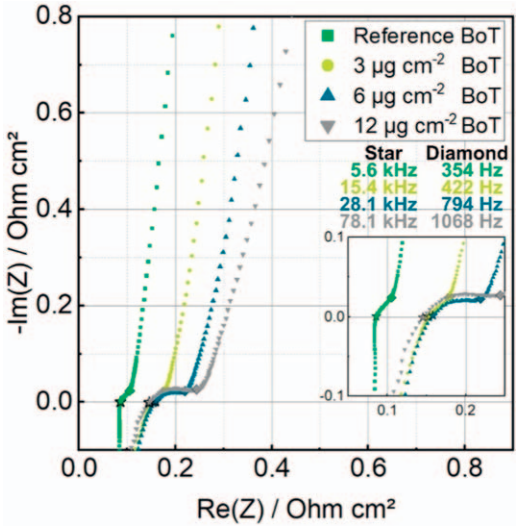

Figure 7. BoT impedance analysis at blocking conditions of the reference MEA and the three different MEAs containing composite membranes with different GO loadings as interlayers at 50 °C cell temperature, a flow rate of 0.1 l min^{-1} hydrogen, and 0 ml min^{-1} DI water feed. Depicted are the impedance analyses of one MEA per sample type.

the Nafion membrane and therefore slightly reduce the membrane thickness and thereby also the HFR.

TEM analysis was performed before and after the acetone hydrogenation experiments to investigate a possible rearrangement in the GO-blocking interlayer. The results can be seen in Fig. 9c. While the GO interlayer in the pristine state (Fig. 9c, pristine membrane) presents an ordered and homogenous structure (see locally increased carbon and oxygen EDX signals at the GO interlayer) within the Nafion matrix (see fluorine EDX signal), the GO flakes seem to rearrange and build a clustered structure after the acetone hydrogenation experiments (Fig. 9c post-mortem). These results additionally support the conclusion that GO interlayer undergoes a rearrangement during operation, which decreases the additional interface resistance and increases the membrane's proton conductivity.

All MEAs show a reduced OCV at EoT compared with BoT (compare Table I). However, the blocking layers appear to maintain their function as a permeation barrier since the absolute values are higher than those of the reference (up to 12% higher OCV for the 6 and 12 µg cm^{-2} GO MEA compared to the reference MEA), and the relative losses in OCV decrease with increasing GO loading (e.g., approx. 6% lower OCV at EoT vs BoT for the reference, but less than 3% lower OCV for the 12 µg cm^{-2} interlayer sample). Thus, the crossover through the GO containing composite membranes, which is a main driver of lower OCV compared to the theoretical reversible cell potential, is still reduced at EoT, despite the observed rearrangement of the interlayer throughout the test. We attribute the generally observed decrease in OCV to an increase in thermally catalyzed acetone hydrogenation with the hydrogen crossover. We assume an elevated thermal catalytic activity for the metallic Pt-Ru sites at EoT in comparison to the partial oxides and hydrous oxides at BoT. The increased thermally catalyzed conversion of acetone to isopropanol reduces the reversible potential according to the Nernst equation. Furthermore, an increased apparent hydrogen crossover is measured in 1 M acetone at EoT (see Fig. 10a), while the crossover in DI water remains constant or even decreases (Fig. 10b). The increase in hydrogen crossover measured in acetone can on the one hand be attributed to the increased swelling of the membrane in acetone and thereby opening-up of pathways for hydrogen, and on the other hand to an increased HOR activity of the reduced

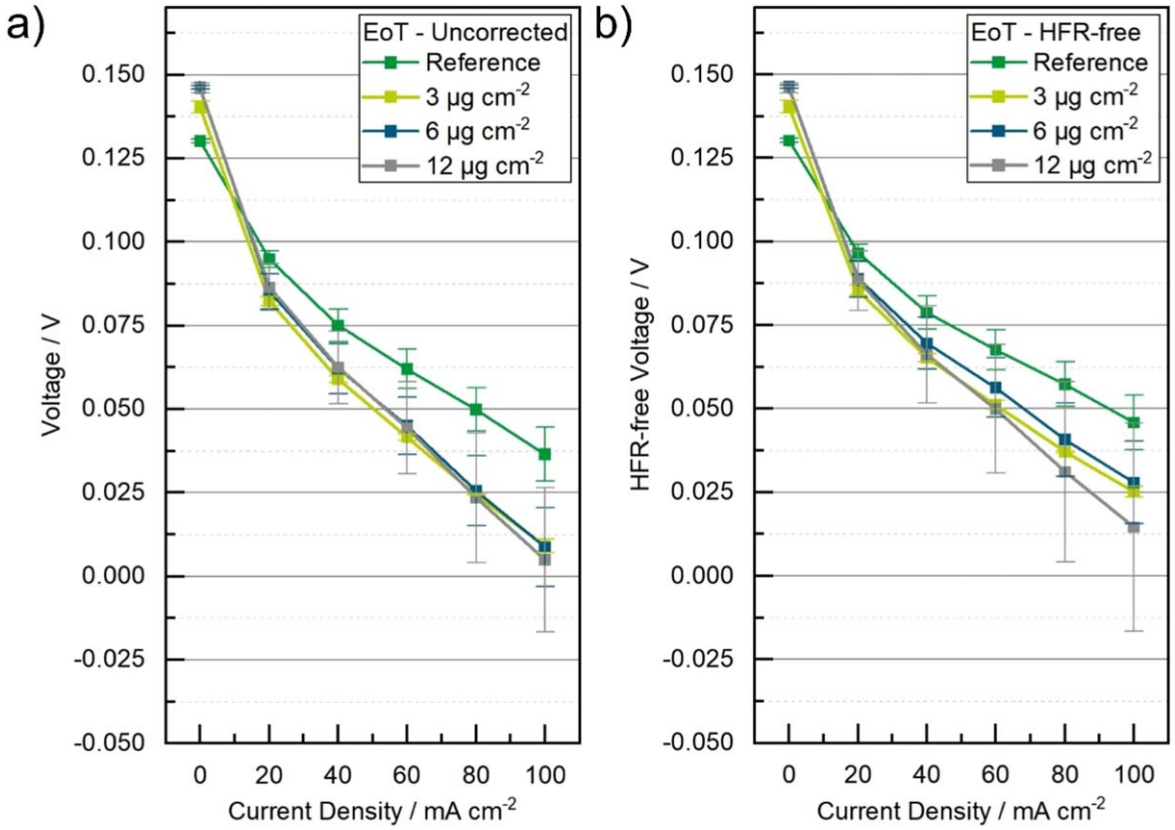

Figure 8. Uncorrected (a) and HFR-free (b) polarization curves at EoT for the reference and the three different GO interlayer loadings. The polarization data were acquired at 50 °C cell temperature, 1 M acetone, a flow rate of 0.1 l min^{-1} hydrogen, and 7.5 ml min^{-1} acetone feed. Depicted are the means of two MEAs for each data point, with the error bars indicating the minimum and maximum. A line between the single data points is added to guide the eye.

Pt-Ru sites at EoT compared to BoT. From the experiments we assume that the activity towards the HOR in the crossover measurement and the thermally catalyzed acetone hydrogenation reaction are both increased at EoT, but since the reaction rate for the HOR is presumably faster, higher hydrogen crossover currents can be measured at EoT than at BoT. This is due to a larger portion of hydrogen being electrochemically oxidized before being available for the thermal acetone hydrogenation reaction. In total, this leads to an increased apparent hydrogen crossover at EoT in comparison to BoT. The electrochemical determination of hydrogen crossover, in the presence of acetone, remains challenging due to the contesting electrochemical and thermocatalytic reactions taking place in the system. Nevertheless, the stability of the hydrogen crossover at BoT vs EoT measured in DI water, which is free of those competing reactions, confirms the durability of the GO interlayers.

Furthermore, the permeation of organics (Fig. 10c) was quantified at EoT. While the absolute permeation of organics for all three GO loaded membranes remains in the error range throughout testing, the organic permeation rate of the reference indicates a decrease when comparing BoT and EoT. As observed in Fig. 3b, we attribute the decrease in organic permeation for the reference MEAs to measurement deviations. Nevertheless, the reduction in the organic crossover of the MEAs with GO interlayer remains observable for the MEAs with the 6 and 12 µg cm^{-2} GO interlayers compared to the reference's permeation behavior at EoT. The comparison of the BoT and EoT organic permeation rate, including a third repetition for the reference, 3 and 12 µg cm^{-2} GO interlayer MEAs can be seen in the supporting information (Fig. S8). Those results indicate that the permeation properties of the reference MEA remain constant within the error bars throughout the testing procedure when increasing the number of measurement repetitions. Thus, these results underline the stable reduction of organic permeation for all three tested GO interlayer loadings at EoT, supporting the durability of the GO interlayer's blocking ability. Since the hydrogen crossover rate measured in water remains constant throughout testing for all three GO loadings and the reference MEA, we conclude that the barrier function of the GO interlayer stays intact also after running the acetone hydrogenation reactor at challenging operating conditions such as high temperatures up to 80 °C.

Conclusions

This work introduces a GO composite membrane for application in an acetone hydrogenation PEM reactor. In-depth electrochemical and offline analysis reveals significant suppression of organic permeation and hydrogen crossover. The blocking effect of the GO interlayers is accompanied by an increase in OCV. Impedance analysis suggests an increased HFR due to the GO interlayer and shows an additional RC element-like feature in the spectra when introducing the GO layer. The changes in the impedance spectra highlight the complexity of an adequate electrochemical analysis of composite membranes and the comparison with reference materials, which is insufficiently represented by only interpreting a simple HFR value. Notably, the additional feature in the impedance spectra diminished throughout the about net 15 h lasting electrochemical testing protocol, which indicates morphological changes occur in the membrane significantly below its glass transition temperature, even within only a few hours of operation. Nonetheless, the effect of the GO blocking interlayer was maintained even after running the acetone hydrogenation reactor at demanding conditions, highlighting its potential as a durable interlayer. Besides these promising results, the trade-off of a non-proton

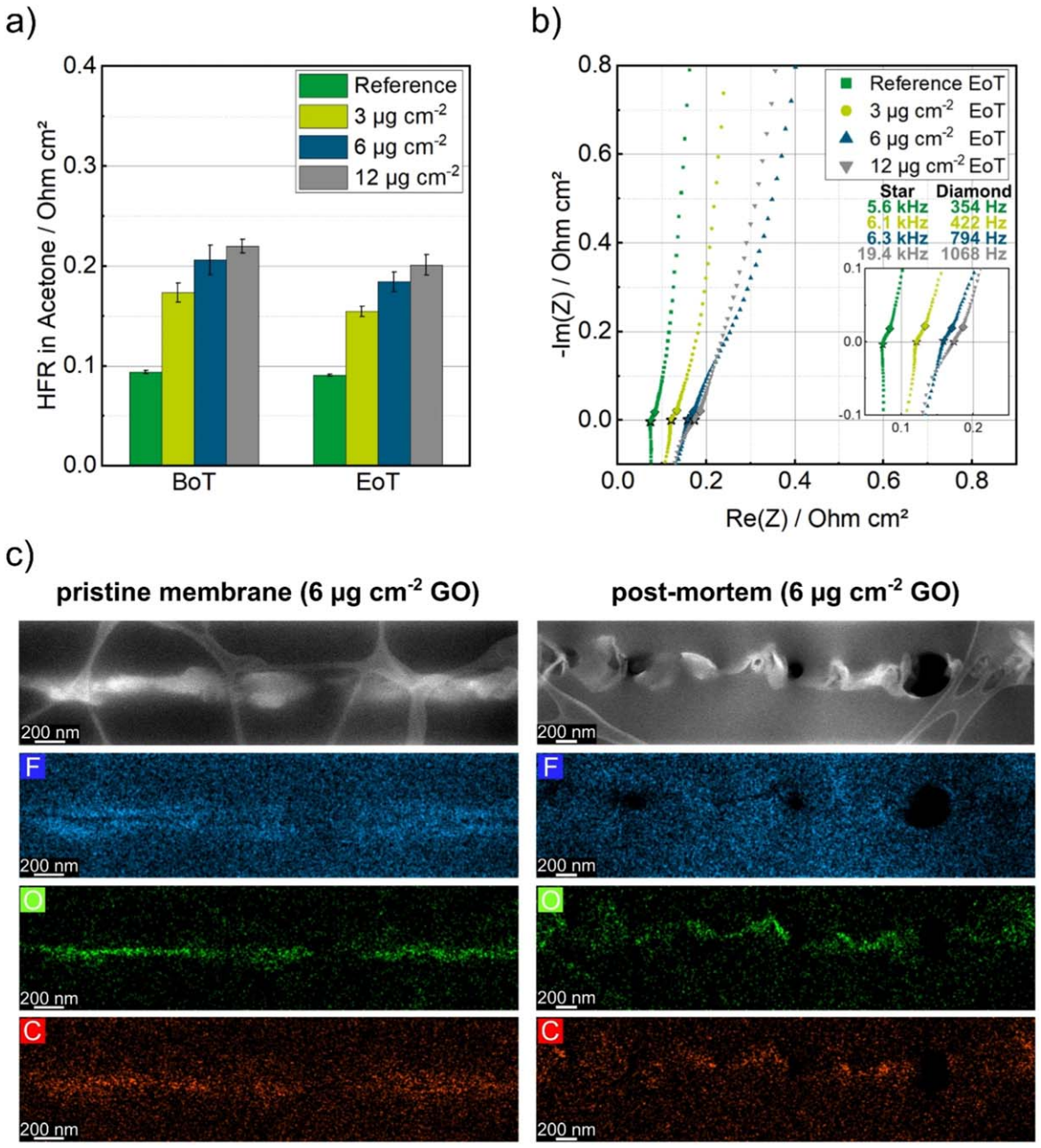

Figure 9. (a) BoT and EoT comparison of the HFR values measured in 1 M acetone with 0.1 l min^{-1} hydrogen flow and 0 l min^{-1} acetone feed at 50 °C. Depicted are the means of two MEAs for each analysis, with the error bars indicating the minimum and maximum; (b) EoT impedance analysis at blocking conditions of the reference MEA and the three different MEAs containing composite membranes with different GO loadings as interlayers at 50 °C cell temperature, a flow rate of 0.1 l min^{-1} hydrogen, and 0 ml min^{-1} DI water feed. Depicted are the impedance analyses of one MEA each, containing a composite membrane and one reference MEA; (c) TEM analysis of a pristine membrane with a GO loading of 6 µg cm^{-2} and an MEA after the electrochemical acetone hydrogenation experiments. The upper panel shows the HAADF-STEM (high-angle annular dark field scanning transmission electron microscopy) signal and the lower three panels EDX signals. The EDX signal for fluorine (F) is shown in blue, representing the Nafion matrix, while the GO interlayer is represented by the locally increased intensity in the green oxygen (O) signal and the red carbon (C) signal. The fibrous structures visible in the HAADF-STEM images originate from the lacey carbon coating of the employed Cu grids. Dark spots within the images indicate image artifacts caused by beam damage.

conductive layer in a PEM must be considered: lower reactant crossover is inevitably linked to a lower proton conductivity as well. The reduced proton conductivity of the GO composite membrane would lead to drastic performance losses in electrochemical systems that are dominated by ohmic losses, like low-temperature PEM fuel cells. In contrast, the acetone hydrogenation reactor operates at lower current densities due to sluggish reaction kinetics, which results in a dominating dependency on conversion efficiency rather than ionic conductivity through the membrane. Hence, blocking interlayers such as the herein introduced GO interlayer not only have to be fine-tuned in terms of ideal loading to reach the best compromise between permeation reduction and maintained membrane conductivity but also be adapted to the desired use case. PEM-based electrochemical cells that operate with organics such as alcohols are prone to high reactant crossover rates, which can be effectively counteracted with a blocking interlayer such as GO flakes.

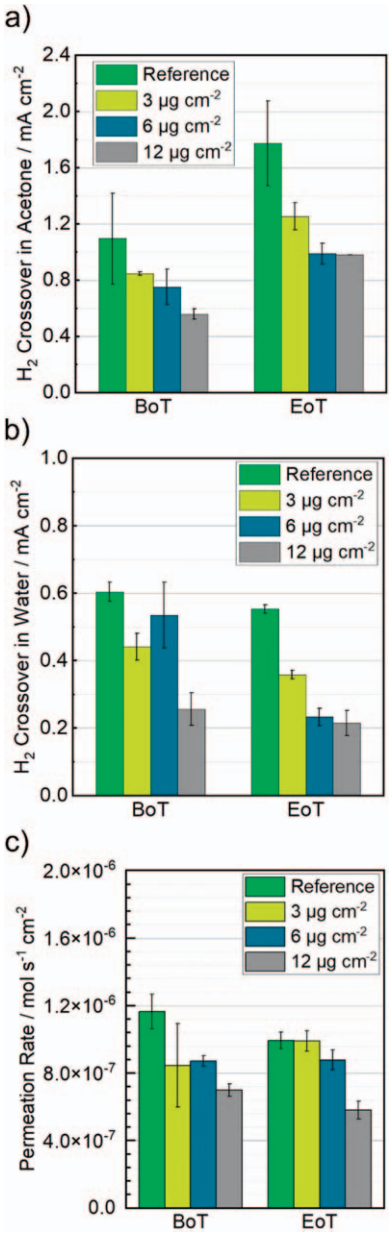

Figure 10. H_2 crossover currents measured at 50 °C via voltage stepping at a flow rate of 0.1 l min^{-1} hydrogen and 0 l min^{-1} of (a) 1 M acetone or (b) DI water; (c) the permeation rate of organic species from the cathodic compartment to the anodic compartment. The crossover of organics was determined during a 15 min hold at OCV with a flow rate of 0.1 l min^{-1} hydrogen and 7.5 ml min^{-1} of 1 M acetone at 50 °C. Depicted are the means of two MEAs for each analysis, with the error bars indicating the minimum and maximum.

Acknowledgments

The authors gratefully acknowledge the financial support of this work by the Federal Ministry of Education and Research in Germany within the project PowerMem (grant number 03EW0012A). The authors declare no conflict of interest. The overall conceptualization, experimental conception, identification of key challenges, and conduction and analysis of experiments were done by M.K and A. M. Scientific discussion and experimental support were provided by T.B, M.M, and A.H. M.M performed Raman measurements and analysis. T.B prepared cross-sections for the TEM analysis. A.H conducted the TEM measurement and analysis. The supervision of the project was done by T.B and S.T. The publication was proofread and commented by all authors.

ORCID

Miriam Komma https://orcid.org/0000-0002-3062-1380
Andreas Hutzler https://orcid.org/0000-0001-5484-707X
Thomas Böhm https://orcid.org/0000-0003-2036-2159
Simon Thiele https://orcid.org/0000-0002-4248-2752

References

1. G. S. Seck et al., *Renew. Sustain. Energy Rev.*, **167**, 112779 (2022).
2. A. M. Elberry, J. Thakur, A. Santasalo-Aarnio, and M. Larmi, *Int. J. Hydrog. Energy*, **46**, 15671 (2021).
3. N. Rusman and M. Dahari, *Int. J. Hydrog. Energy*, **41**, 12108 (2016).
4. M. Brodt, K. Müller, J. Kerres, I. Katsounaros, K. Mayrhofer, P. Preuster, P. Wasserscheid, and S. Thiele, *Energy Technol.*, **9**, 2100164 (2021).
5. J. Cho, B. Kim, S. Venkateshalu, D. Y. Chung, K. Lee, and S.-I. Choi, *J. Am. Chem. Soc.*, **145**, 16951 (2023).
6. K. Matsuoka, K. Miyoshi, and Y. Sato, *J. Power Sources*, **343**, 156 (2017).
7. C. Li, A. Sallee, X. Zhang, and S. Kumar, *Energies*, **11**, 2691 (2018).
8. P. Hauenstein, D. Seeberger, P. Wasserscheid, and S. Thiele, *Electrochem. Commun.*, **118**, 106786 (2020).
9. P. Hauenstein, I. Mangoufis-Giasin, D. Seeberger, P. Wasserscheid, K. J. Mayrhofer, I. Katsounaros, and S. Thiele, *Journal of Power Sources Advances*, **10**, 100064 (2021).
10. S. M. Holmes, P. Balakrishnan, V. S. Kalangi, X. Zhang, M. Lozada-Hidalgo, P. M. Ajayan, and R. R. Nair, *Adv. Energy Mater.*, **7**, 1601216 (2017).
11. T. Yuan, L. Pu, Q. Huang, H. Zhang, X. Li, and H. Yang, *Electrochim. Acta*, **117**, 393 (2014).
12. H.-C. Chien, L.-D. Tsai, C.-P. Huang, C. Kang, J.-N. Lin, and F.-C. Chang, *Int. J. Hydrog. Energy*, **38**, 13792 (2013).
13. C. Götz, M. Komma, D. Dworschak, S. Thiele, and T. Böhm, *Adv. Mater. Interfaces*, **11**, 2300887 (2024).
14. I. Shabani, M. M. Hasani-Sadrabadi, V. Haddadi-Asl, and M. Soleimani, *J. Membr. Sci.*, **368**, 233 (2011).
15. X. H. Yan, R. Wu, J. B. Xu, Z. Luo, and T. S. Zhao, *J. Power Sources*, **311**, 188 (2016).
16. S. Lee, W. Jang, M. Kim, J. E. Shin, H. B. Park, N. Jung, and D. Whang, *Small*, **15**, e1903705 (2019).
17. H. S. Thiam, W. Daud, S. K. Kamarudin, A. B. Mohamad, A. Kadhum, K. S. Loh, and E. H. Majlan, *Energy Convers. Manage.*, **75**, 718 (2013).
18. M. Breitwieser, T. Bayer, A. Büchler, R. Zengerle, S. M. Lyth, and S. Thiele, *J. Power Sources*, **351**, 145 (2017).
19. G. G. Gagliardi, A. El-Kharouf, and D. Borello, *Fuel*, **345**, 128252 (2023).
20. S. Claramunt, A. Varea, D. López-Díaz, M. M. Velázquez, A. Cornet, and A. Cirera, *J. Phys. Chem. C*, **119**, 10123 (2015).
21. T. Böhm, R. Moroni, M. Breitwieser, S. Thiele, and S. Vierrath, *J. Electrochem. Soc.*, **166**, F3044 (2019).
22. S. Hikita, *JSAE Review*, **22**, 151 (2001).
23. S. H. Seo and C. S. Lee, *Appl. Energy*, **87**, 2597 (2010).
24. Z. Yang, W. Chen, J. Zheng, Z. Yang, N. Zhang, C.-J. Zhong, and B. H. Chen, *J. Catal.*, **363**, 52 (2018).
25. S. A. Vilekar and R. Datta, *J. Power Sources*, **195**, 2241 (2010).
26. A. Kusoglu and A. Z. Weber, *Chem. Rev.*, **117**, 987 (2017).
27. K. C. Neyerlin, W. Gu, J. Jorne, A. Clark, and H. A. Gasteiger, *J. Electrochem. Soc.*, **154**, B279 (2007).
28. N. C. Röttcher, Y.-P. Ku, M. Minichova, K. Ehelebe, and S. Cherevko, *J. Phys.: Energy*, **5**, 24007 (2023).
29. Y. Ji, M. Hou, Y. Zheng, W. Chen, and Z. Wang, *Colloids Surf., A*, **561**, 292 (2019).
30. D. R. Rolison, P. L. Hagans, K. E. Swider, and J. W. Long, *Langmuir: The ACS Journal of Surfaces and Colloids*, **15**, 774 (1999).